

## Supplementary Methods

### NIR fluorescent tracer: bevacizumab-800CW

#### Tracer production and administration

Clinical grade bevacizumab-800CW was produced at the University Medical Centre Groningen (UMCG, Groningen, the Netherlands), according to good manufacturing practice (GMP) guidelines (1). The labelling of the monoclonal antibody bevacizumab (Avastin<sup>®</sup>, Roche, Hertfordshire, United Kingdom) with the near infrared (NIR) fluorophore IRDye 800CW (IRDye800CW-NHS ester; LI-COR Biosciences, Lincoln, NE, USA) was performed in a 4:1 or 2:1 dye-to-protein [D:P] molar ratio in a phosphate-buffered saline (PBS, pH 8.5) solution (Table S1). The D:P molar ratio was lowered from 4:1 to 2:1 to guarantee stability of tracer compound. The lower ratio was administered in the 10 mg and 25 mg groups [1-3] .

After conjugation, the product was purified by buffer exchange, formulated, passed over a sterile 0.2 µm filter and filled into injection vials (1 mg/mL). During and after production, quality control was performed to assess identity, chemical quality, chemical purity and biological activity of the tracer. Endotoxin levels and bioburden were assessed in accordance with the European Pharmacopoeia 8.0. Labelling efficiency, theoretical D:P molar ratio, quality and purity were determined by a validated size-exclusion high-performance liquid chromatography (SE-HPLC) method (Table S1). Bevacizumab-800CW was infused intravenously (IV; infusion rate 75 mL/h) three days before the surveillance endoscopy. This time interval was chosen based on experience with <sup>89</sup>Zr-bevacizumab PET-scans in renal cell cancer patients [4]. Patients were observed during one hour, with close monitoring of blood pressure, pulse and temperature. Based on the toxicity study of cetuximab-800CW in cynomolgus macaques, which showed increased QTc time, and in-human results regarding elevated levels of aspartate aminotransferase (AST), patients included in the 10 and 25 mg dose groups also received an ECG and baseline routine blood levels (full blood count, serum creatinine, liver enzymes, magnesium, calcium and β-HCG in women of childbearing potential), prior to infusion of the tracer [5, 6] .

### Near-infrared fluorescence molecular endoscopy (NIR-FME)

#### Probe-based NIR-FME system

The NIR-FME system (Surgvision, 't Harde, the Netherlands) is developed in such a way that it can be easily incorporated in clinical endoscopy procedures. It is a probe-based system, making use of a custom-made Micrendo<sup>®</sup> fiber bundle, containing 30,000 coherently-arranged individual fibres (Schölly Fiberoptic GmbH,

Denzlingen, Germany). The fibre bundle has a field of view of 85° and a diameter of 2.4 mm, making it suitable for insertion through the working channel of a commercially available video endoscope. White-light illumination of the fibre was provided by a LED light source (KL 2500 LED, Schott AG, Mainz, Germany) with a shortpass dichroic filter (E700SP-2P; Chroma, Bellows Falls, VT, USA). Fluorescence excitation was achieved by two class IIIb lasers (750nm, max. power 300 mW; BWF1, B&WTEK, Newark, DE, USA). Both light sources are coupled to the fibre bundle via a multi-branched fibre-optic bundle (SEDI-ATI Fibres Optiques, Courcouronnes, France). The fibre bundle itself is connected to a mechanical and focusing adapter (Schölly Fiberoptic, Denzlingen, Germany). This connection conducts the fibre images via a dichroic mirror and bandpass filter (819 nm,  $\pm 44$  nm, Semrock inc, Rochester, NY, USA) to a charge-coupled digital (EM-CCD) camera, sensitive for NIR light, and a separate camera for colour detection (Figure S1A). The cameras are installed at a movable arm with two swivel joints. The software generates an overlay image of both cameras and projects this real-time during the procedure on a second screen. In this way, fluorescence molecular guidance is realized with little impact to current workflow of clinical endoscopy procedures. The performance of the NIR-FME system was characterized as described before, with a spatial resolution of 198.42  $\mu\text{m}$  at a distance of 2 cm, and a detection limit at a concentration of 19.80 nM [7].

## **MDSFR/SFF spectroscopy**

### **Instrument description**

The Multi Diameter Single Fiber Reflectance and Single Fiber Fluorescence (MDSFR/SFF) spectroscopy device uses an optical fibre probe, consisting of two adjacent optical fibres with different diameters (0.4 and 0.8 mm). White-light from a tungsten halogen lamp (HL-2000-FHSA; Ocean Optics, Duiven, NL), was directed through these fibres, for the sequential acquisition of a reflection measurements using two spectrometers (SD-2000; Ocean Optics). Subsequently, 775 nm laser light was directed through the 0.8 mm fibre to obtain a fluorescence spectrum using a separate sensitive spectrometer (QE-65000; Ocean Optics). A long pass filter (785 nm) was used to block scattered excitation light (Figure S1B). The tip of the probe has an angle of 15° to minimize internal specular reflections. Spectrometers and light sources were controlled by a custom made LabView program (LabView 7.1; National Instruments Corporation, Austin, TX, USA) as described previously [8,9]. Before every procedure, a calibration was performed to correct for fibre alignment and transmission efficiency, using a 1.3% intralipid phantom [10]. An *ex vivo* MDSFR/SFF spectroscopy measurement took approximately 3 sec per location.

### Spectral fitting and the determination of intrinsic fluorescence

The MDSFR/SFF spectroscopy device was used to quantify the NIR fluorescent signals of the freshly resected colorectal tissue. The approach is based on the measurement of multiple, in the case of the current study, two single fibre reflectance spectra. From these spectra the wavelength dependence of the reduced scattering coefficient  $\mu'_s$  and the parameter  $\gamma(\lambda)$ , which is related to the angular distribution of light scattering in tissue, is determined. It is then possible to determine the absorption coefficient  $\mu_a(\lambda)$  of the tissue based on a set of specific chromophores: bilirubin, oxygenated haemoglobin and deoxygenated haemoglobin. By combining the measurements of the tissue optical properties ( $\mu'_s$  and  $\mu_a$ ) at both the fluorescence excitation wavelength (775 nm) and the fluorescence emission wavelength range of the tracer (780 – 850 nm) with a measurement of the raw fluorescence from the tissue, it is possible to recover the intrinsic fluorescence  $Q \cdot \mu_{a,x}^f$ . The intrinsic fluorescence  $Q \cdot \mu_{a,x}^f$  is defined as the product of the quantum efficiency across the emission spectrum,  $Q[-]$ , where  $Q$  is the fluorescence quantum yield of IRDye 800CW and  $\mu_{af} [\text{mm}^{-1}]$  is the tracer absorption coefficient at the excitation wavelength. The methodology of the determination of the correction factor has been previously described in detail [9]. Quantitative fluorescence spectra were fitted as a linear combination of background autofluorescence basis spectra, determined from adenomatous polyps of a FAP patient that had not received the fluorescent tracer and average basis spectra formed from two patients that received the highest dose of tracer (25 mg). To overcome the problem of noise in the fluorescence signal between 780 and 790 nm (where our detection filter blocks both scattered excitation and fluorescence light) and to satisfy our intention to include the whole of the emission spectrum in the calculation of  $Q \cdot \mu_{a,x}^f$ , we utilized a spectrum of bevacizumab-800CW in PBS to fit spectral data below 790 nm.

Figure S2A and S2B show the measured reflection spectra of two LGD adenomas, both derived from the 25 mg dose cohort. In adenoma A the estimated optical properties are  $\mu'_s(\text{at } 775 \text{ nm}) = 2.53 \text{ mm}^{-1}$  and  $\mu_a(\text{at } 775 \text{ nm}) = 0.0004 \text{ mm}^{-1}$  and of adenoma B  $\mu'_s(\text{at } 775 \text{ nm}) = 0.61 \text{ mm}^{-1}$  and  $\mu_a(\text{at } 775 \text{ nm}) = 0.0087 \text{ mm}^{-1}$ . The characteristic wavelength dips around 400 nm and between 500-600 nm are caused by the strong absorbance properties of haemoglobin. When comparing the reflectance spectra of both adenomas, note the significantly higher reflectance over the whole wavelength range in adenoma A (0.8 mm diameter fibre; blue). This is because this polyp contained significantly less haemoglobin compared to adenoma B, which clearly shows the characteristic double absorption dip centred on 575 nm due to oxygenated haemoglobin. The measured raw fluorescence was subsequently corrected for the estimated optical properties to yield the intrinsic fluorescence

$Q \cdot \mu_{a,x}^f$ . Adenoma B needed a higher correction factor to yield the intrinsic fluorescence because of the higher light absorption by oxygenated haemoglobin. That the tissue optical properties differed over all tissue samples, is reflected in the correction factor that ranged from 1.65 to 3.57. Figure S2C shows a representative example of an intrinsic fluorescence spectrum (and its fit in blue). The *in vivo* fluorescence spectrum closely resembles the fluorescence spectrum of bevacizumab-800CW in PBS (data not shown).

### **Determination of bevacizumab-800CW concentration**

In the calculations of in-tissue bevacizumab-800CW concentration, we assumed that all IRDye800CW fluorescence originated of intact bevacizumab-800CW. With knowledge of the intrinsic fluorescence,  $Q \cdot \mu_{a,x}^f$ , it is interesting to determine an estimation of the actual concentration of bevacizumab-800CW present in the tissue. To estimate its extinction at 775 nm, we first acquired an absorption spectrum of bevacizumab-800CW (D:P molar ratio of 2:1, in 50 mM phosphate NaCl) (Figure S2D). From this, we calculated the extinction coefficient of bevacizumab-800CW at 775 nm of approximately  $311,204 \text{ M}^{-1} \text{ mm}^{-1}$ . The best available data in the literature suggests that fluorescence quantum yield of IRDye800CW is 0.09 [11]. When we assume that the extinction coefficient as well as the fluorescence quantum yield are representative for the *in vivo* conditions, we can calculate the tissue tracer concentration by dividing the intrinsic fluorescence  $Q \cdot \mu_{a,x}^f$  by the extinction coefficient and the fluorescence quantum yield. Under these assumptions, the median measured bevacizumab-800CW concentration in LGD adenomas after the IV administration of 25mg was  $6.86 \text{ nmol mL}^{-1}$ .

## ***Ex vivo* signal analyses**

### **NIR fluorescence flatbed scanner**

The Odyssey CLx imaging system (LI-COR Biotechnology, Lincoln, NE, USA) is a NIR fluorescence flatbed scanner. It contains a solid-state laser diode to excite at 785 nm and silicon avalanche photodiodes to detect at 800 nm, creating high quality and resolution NIR fluorescence images (laser intensity set at 6; spatial resolution of 21  $\mu\text{m}$ , focus 0 mm, scanning speed 5 cm/s).

### **Immunohistochemical analysis of VEGFA expression**

At start, 4  $\mu\text{m}$  FFPE tissue sections were deparaffinised and rehydrated. Heat-induced antigen retrieval was performed with citrate buffer (10mM, pH 6.0; 15 min microwave), followed by endogenous peroxidase blocking with 1.5 mL 30% hydrogen peroxide in 48.5 mL PBS (30 min). After PBS washing steps, the sections

were incubated overnight at 4°C with polyclonal rabbit anti-human VEGFA (RB9031; Thermo Fisher Scientific, Waltham, MA, USA; 0.2 µg/mL, dissolved 1:300 in PBS with 1% bovine serum albumin (BSA)). Tissue was stained using goat-anti-rabbit-HRP IgG (DAKO, Glostrup, Denmark; 1:50 in PBS, 1% BSA, 1% antibody serum) for 30 min at room temperature, followed by rabbit-anti-goat-HRP (DAKO; 1:50 in PBS, 1% BSA, 1% antibody serum). Visualization took place with diaminobenzidine (DAB) for 10 min. Finally, the sections were counterstained with Mayer's haematoxylin, dehydrated and mounted with a glass cover slip. Dysplastic crypts, normal crypts in the adenoma sections and biopsy derived normal mucosa were scored separately for their staining intensity (0-3 scale) and the percentage of cells stained. This visual scoring was performed by two observers (JJJT and EH). Subsequently, H-scores were generated (continuous scale: 0-300) by combining the evaluated intensity and the corresponding percentage of cells stained (formula used:  $1x$  (percentage of cells weakly stained [1+]) +  $2x$  (percentage of cells moderately stained [2+]) +  $3x$  (percentage of cells strongly stained [3+]), creating expression categories representative for overall protein expression per tissue type (0-100 = negative/low; 101-200 = intermediate; 201-300 = high) [12].

### Supplementary references

1. ter Weele EJ, Terwisscha van Scheltinga AGT, Linssen MD, et al. Development, preclinical safety, formulation, and stability of clinical grade bevacizumab-800CW, a new near infrared fluorescent imaging agent for first in human use. *Eur J Pharm Biopharm.* 2016; 104: 226–234.
2. Cohen R, Stammes MA, de Roos IH, et al. Inert coupling of IRDye800CW to monoclonal antibodies for clinical optical imaging of tumor targets. *EJNMMI Res.* 2011; 1:31.
3. Cohen R, Vugts DJ, Walsum MS-V, et al. Inert coupling of IRDye800CW and zirconium-89 to monoclonal antibodies for single- or dual-mode fluorescence and PET imaging. *Nat Protoc.* 2013; 8: 1010–1018.
4. Oosting SF, Brouwers AH, van Es SC, et al. <sup>89</sup>Zr-Bevacizumab PET visualizes heterogeneous tracer accumulation in tumor lesions of renal cell carcinoma patients and differential effects of antiangiogenic treatment. *J Nucl Med.* 2015; 56: 63–69.
5. Zinn KR, Korb M, Samuel S, et al. IND-directed safety and biodistribution study of intravenously injected cetuximab-IRDye800 in cynomolgus macaques. *Mol Imaging Biol.* 2015; 17: 49–57.
6. Rosenthal EL, Warram JM, de Boer E, et al. Safety and tumor specificity of cetuximab-IRDye800 for surgical navigation in head and neck cancer. *Clin Cancer Res.* 2015; 21: 3658–3666.
7. Tjalma JJJ, Garcia-Allende PB, Hartmans E, et al. Molecular fluorescence endoscopy targeting vascular

- endothelial growth factor A for improved colorectal polyp detection. *J Nucl Med.* 2016; 57: 480–485.
8. van Leeuwen-van Zaane F, Gamm UA, van Driel PBAA, et al. Intrinsic photosensitizer fluorescence measured using multi-diameter single-fiber spectroscopy in vivo. *J Biomed Opt.* 2014; 19: 1560-2281.
  9. Middelburg TA, Hoy CL, Neumann HAM, et al. Correction for tissue optical properties enables quantitative skin fluorescence measurements using multi-diameter single fiber reflectance spectroscopy. *J Dermatol Sci.* 2015; 79: 64–73.
  10. Hoy CL, Gamm UA, Sterenborg HJCM, et al. Use of a coherent fiber bundle for multi-diameter single fiber reflectance spectroscopy. *Biomed Opt Express.* 2012; 3: 2452–2464.
  11. Leung K. IRDye 800CW-Human serum albumin. *MICAD.* 2012; 102: 107–112.
  12. Hirsch FR, Varella-Garcia M, Bunn PA, et al. Epidermal growth factor receptor in non-small-cell lung carcinomas: correlation between gene copy number and protein expression and impact on prognosis. *J Clin Oncol.* 2003; 21: 3798–3807.

**Table S1. Tracer production characteristics.**

<b>Dose group</b>	<b>D:P<sup>A</sup></b>	<b>Labelling efficiency (%)</b>	<b>Theoretical D:P</b>
4.5 mg	4:1	80 %	3.20:1
10 and 25 mg	2:1	83.4 %	1.67:1

<sup>A</sup>Dye-to-protein molar labelling ratio

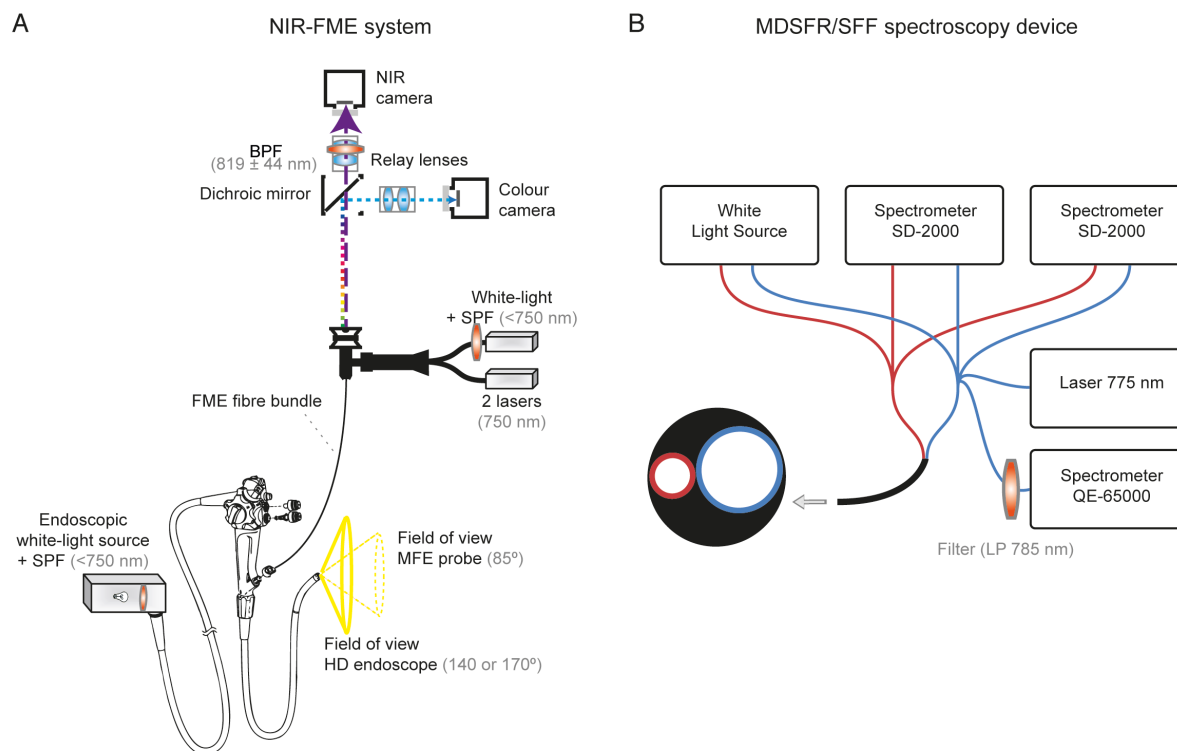


**Figure S1. Schematic representation of the NIR-FME system and the MDSFR/SFF spectroscopy device.**

(A) Fluorescence excitation is provided by two laser sources (750 nm); fluorescence and white-light detection is simultaneously derived by a charge-coupled digital (EM-CCD) NIR camera and a colour camera. The optical fibre bundle is inserted through the working channel of a clinical HD endoscope, creating wide-field FME. (B) Reflection spectra are measured by the two bundled optical fibres ( $\varnothing$  0.4 and 0.8 mm), followed by one fluorescence spectrum measurement via the largest fibre ( $\varnothing$  0.8 mm, 775 nm fluorescence excitation light). NIR, near-infrared; HD, high definition; FME, fluorescence molecular endoscopy; BPF, band pass filter; SPF, short pass filter.

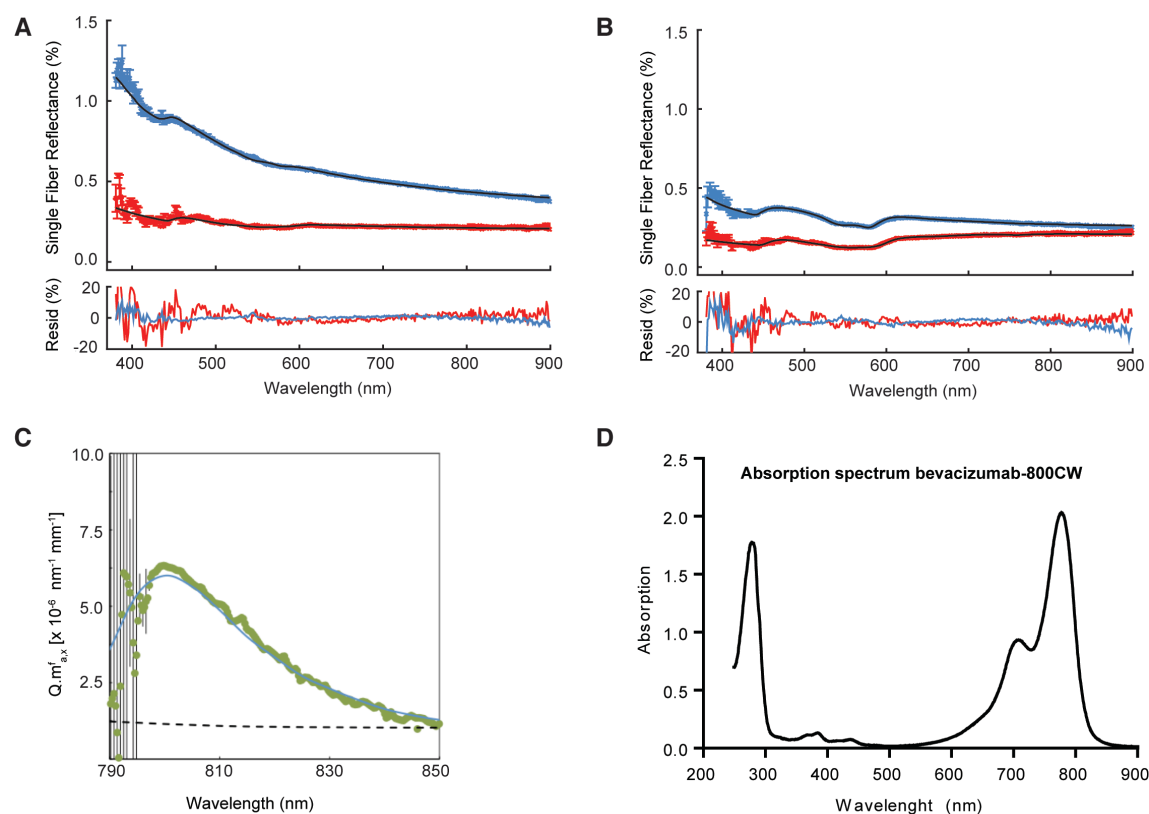


**Figure S2. MDSFR/SFF spectroscopy.** (A-B) Two examples of MDSFR spectra measured for two resected colorectal adenomas with LGD. The percentage of reflected light is plotted against wavelength, blue for the large fibre ( $\varnothing$  0.8 mm) and red for the small fibre ( $\varnothing$  0.4 mm) plus standard deviations. The larger fibre measurement always shows a higher reflectance compared to the smaller fibre due to the larger collection area. Underneath, the corresponding residual lines are plotted to show the difference between the mathematical fit and the actual data. Both fibres show a higher percentage of noise in the lower and higher wavelengths. (C) A representative corrected SFF spectrum of an adenoma from the 25 mg cohort depicted in green. The measured fluorescence is here corrected for the optical properties (tissue absorbance and scattering) calculated from the measured MDSFR spectra. The large error bars around 790 nm are due to the filters applied to block the excitation light. This green spectrum resembles the fluorescence spectrum of bevacizumab-800CW in PBS, which confirms that the measured fluorescent signals are tracer derived. The blue line is the mathematical fit to the data. (D) The absorption spectrum of bevacizumab-800CW dissolved in a 50 mM phosphate NaCl solution. A protein peak is detected at 280 nm and the bevacizumab-800CW absorption peak at 775 nm. This spectrum was used to calculate the absorption coefficient at 775 nm.